applied sciences

MDPI

Article

Superhydrophobic Surfaces Created by Elastic Instability of PDMS

Abbas Sabbah [1,2,*], Ayman Youssef [2] and Pascal Damman [1]

[1] Laboratoire Interfaces et Fluides Complexes, CIRMAP, Université de Mons—UMONS, 20 Place du Parc, B-7000 Mons, Belgium; pascal.damman@umons.ac.be

[2] Environmental Engineering and Natural Resources, Faculty of Agronomy, Lebanese University, Dekouaneh 1203, Lebanon; ayman.youssef@ul.edu.lb

* Correspondence: abbas.sabbah@gmail.com; Tel.: +961-3-464969

Academic Editor: Francisco José Galindo Rosales

Received: 18 February 2016; Accepted: 6 May 2016; Published: 16 May 2016

Abstract: Lotus flowers, rose petals, some plant leaves and insects have a naturally super-hydrophobic surface. In fact, the surface of a Lotus leaf is covered by micro and nano structures mixed with wax, which makes its surface superhydrophobic. In microfluidics, superhydrophobicity is an important factor in the rheometers on a chip. It is also sought in other complex fluids applications like the self-cleaning and the antibacterial materials. The wettability of the surface of solid support can be modified by altering its chemical composition. This means functionalizing the interface molecules to different chemical properties, and/or forming a thin film on the surface. We can also influence its texturing by changing its roughness. Despite considerable efforts during the last decade, superhydrophobic surfaces usually involve, among others, microfabrication processes, such as photolithography technique. In this study, we propose an original and simple method to create superhydrophobic surfaces by controlling elastic instability of poly-dimethylsiloxane (PDMS) films. Indeed, we demonstrate that the self-organization of wrinkles on top of non-wettable polymer surfaces leads to surperhydrophobic surfaces with contact angles exceeding 150°. We studied the transition Wenzel-Cassie, which indicated that the passage of morphology drops "impaled" to a type of morphology "fakir" were the strongest topographies.

Keywords: superhydrophobic surfaces; wetting; microstructures; wrinkles and elastomers

1. Introduction

In recent decades, the study of super-hydrophobicity has become essential in many industrial sectors. From a fundamental point of view, the description of the phenomena of wettability is essentially based on the understanding of the nature of interactions that develop between the liquid and the wet surface. The chemical physics parameters of a surface play an essential role in the wettability properties. By controlling the chemical nature of the surface, we can obtain hydrophobic surfaces. Moreover, using factors which increase the actual contact surface, such as roughness or structure of surfaces can improve it and make it a superhydrophobic surface, which is often sought in the high-technology sectors where self-cleaning surfaces are required [1,2].

To illustrate this, take as example the lotus leaf, which has a natural superhydrophobic surface. Indeed, the surface of the lotus leaf is covered by micro and nano-structures and wax which make it superhydrophobic [3–7]. One of the techniques used for reproducing these structures is based on photolithography. However, lithography is expensive and unsuitable to non-planar system models. So how else can we prepare a super- hydrophobic surface?

Cross-linked poly-dimethylsiloxane (PDMS) has an attractive combination of materials that has flexibility and hydrophobic surface properties [8]. Various approaches have been used to modify

the surfaces of PDMS, including: chemical methods [9–11] and physical methods, such as ultraviolet ozone [12], and oxygen plasma [8,13]. In this paper, we used molding in order to reach the required roughness. Then, we measured the contact angle to determine the degree of hydrophobicity of the hydrophobic film of PDMS. The surface texture of the mold is obtained by a combination of UV/Ozone irradiation and suitable elastic deformation; this process mimics the natural apparition of wrinkles on the human skin.

Human skin is essentially composed of two primary layers: the epidermis, which provides waterproofing and serves as a barrier to infection; and the dermis, which cushions the body from stress and strain. The dermis, whose thickness is about a millimeter, consists of a set of proteins, like collagen fibers, which provide flexibility and elasticity to the skin (Young modulus E is around 0.2–3 MPa). The epidermis is essentially composed of keratinocytes and is much thinner than the dermis with a larger elastic modulus due to its lamellar composition [14]. This difference in elastic modulus, together with aging or compression, yields to wrinkles.

Superhydrophobic surfaces created by elastic instability can contribute to the recent advances in microfluidics which allowed the development of rheometers on a chip [15–17], where microfluidics is a competitive platform for performing rheometry. Therefore, the control of wall adherence and degree of slipping become central topics for this sort of applications application of microfluidics [18–20]. In this sense, the application of superhydrophobic surfaces can potentially help to investigate and analyze the influence of patterned surfaces in microrheometry.

Other potential applications of superhydrophobic surfaces is that they improve coalescence-induced micro-droplet jumping [21], and they can avoid the intensive usage of biocides in antibacterial materials by reducing the bacterial adhesion [22].

2. Materials and Methods

2.1. Preparation of Base Material

Systems used to model the human skin are Sylgard 184 and Sylgard 186 from Dow Corning Inc. (Midland, MI, United States) They are essentially composed of a high viscosity base and a curing agent. Artificial skins are prepared by mixing a ratio 10:1 (base: curing agent), defoaming for 30 min and cross-linking at 75 °C temperature for two hours. The Young moduli, measured with a Mettler Toledo DMA 861e, are estimated around 3 MPa and 1 MPa respectively for Sylgard 184 and 186.

2.2. Method for Fabricating Micro-Wrinkling Pattern

After cross-linking, the PDMS (Sylgard 186) was stretched and oxidized using UV/ozone irradiation for an extended period of time (30–300 min) to increase the number of reticulation points (Figure 1a). The UV/ozone treatment (Applitek PR100, Nazareth, Belguim) changes the surface chemistry of PDMS. It converts the surface of PDMS into a stiff hydrophilic skin, similar to a silicate (SiO_x) layer. After the UV/ozone treatment, the stretching is finally relaxed in order to compress the top layer modeling the epidermis. The compression ratio is defined by [23]:

$$\delta = \frac{L_0 - L}{L_0} \tag{1}$$

Above the threshold for the compression ratio ($\delta > \delta_c$), we observe the formation of sinusoidal wrinkles on the top of the PDMS characterized by a cylindrical symmetry and perpendicular to the direction of the strain.

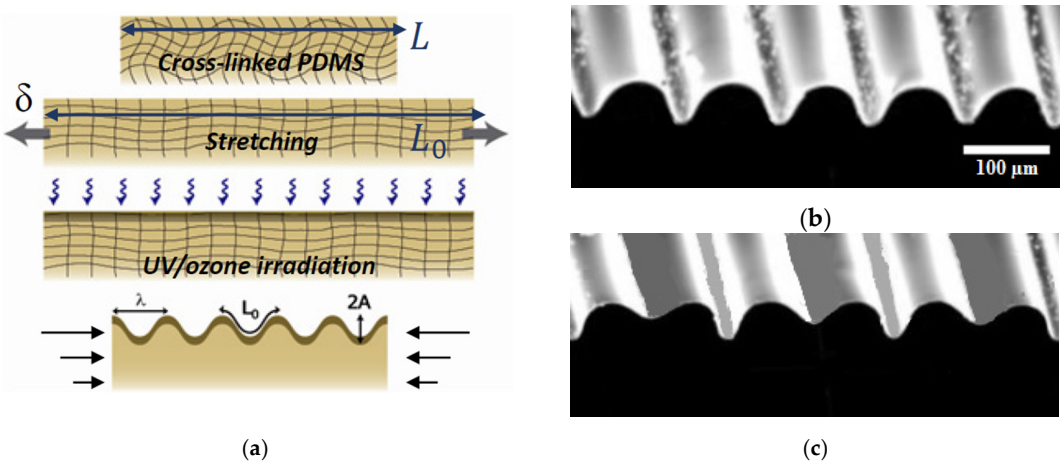

Figure 1. (**a**) Schematics illustrating the steps for fabricating micro-wrinkling pattern on the poly-dimethylsiloxane (PDMS) substrate; (**b**,**c**) Scanning Electron Microscope (SEM) images of wrinkling pattern on a thin stiff PDMS film resting on a thick soft PDMS foundation and obtained with mechanical compression of 28% and 38% respectively.

2.3. Replication of Structured Surface

After UV/ozone treatment, the PDMS surface becomes hydrophilic due to the presence of a silicate-like layer. For small compression, the wrinkles are sinusoidal and characterized by a wavelength λ. For larger compression ratio, periodic folds directed downward in the direction of the elastomer and characterized by a wavelength 2λ emerge. To obtain superhydrophobic surface, those folds should be oriented upward. Consequently, the superhydrophic surfaces are obtained by replica molding the surface with sylgard 184. The large roughness of the surface leads to a superhydrophobic surface.

We tested the hydrophobicity of our surfaces by deposing a millimetric droplet of water (1 μL) on surfaces characterized by three different types of roughness. We also analyzed the behavior with inclined surfaces.

3. Results and Discussion

In order to explain this formation of wrinkles, many theories and experiments have been made over the past 10 years [14,23–29]. The observed wavelength is explained by the balance between the bending energy $U_b \propto Eh^3 \frac{A^2}{\lambda^3}$ of the stiff upper membrane and the stretching energy $U_s \propto E_s A^2$ of the "semi-infinite" foundation. We thus obtain $\lambda \propto h \left(\frac{E}{E_s}\right)^{\frac{1}{3}}$, where E and E_s are respectively the Young modulus of the upper membrane and of the foundation.

The amplitude of the wrinkles is obtained from the inextensibility constraint imposed to the stiff upper membrane: the length of the membrane stays constant during the compression process. This geometric constraint leads to the relation $A \propto \lambda\sqrt{\delta}$.

For the small deformation ($\delta < 0.3\%$), we observed that there is a continuous increase of the amplitude A of the wrinkles and a continuous decrease of the wavelength λ ($\lambda \propto \lambda_0 (1-\delta)$) (Figure 2(a1), (a2), c).

For the large deformation ($\delta > 0.3$), the situation is different. The profile of the thin elastic membrane is no longer described by a simple sinusoidal. A more complex pattern emerges and is characterized by two amplitudes A_1 and A_2 (Figure 2(a3), b, c). The evolution of the amplitudes of the pattern presents a bifurcation above some critical threshold: some wrinkles grow in amplitude while others decrease. The new pattern emerging is now characterized by a wavelength which is double the initial one. The amplitude of the 2λ mode increases with the compression ratio δ, while the amplitude of λ mode vanishes progressively.

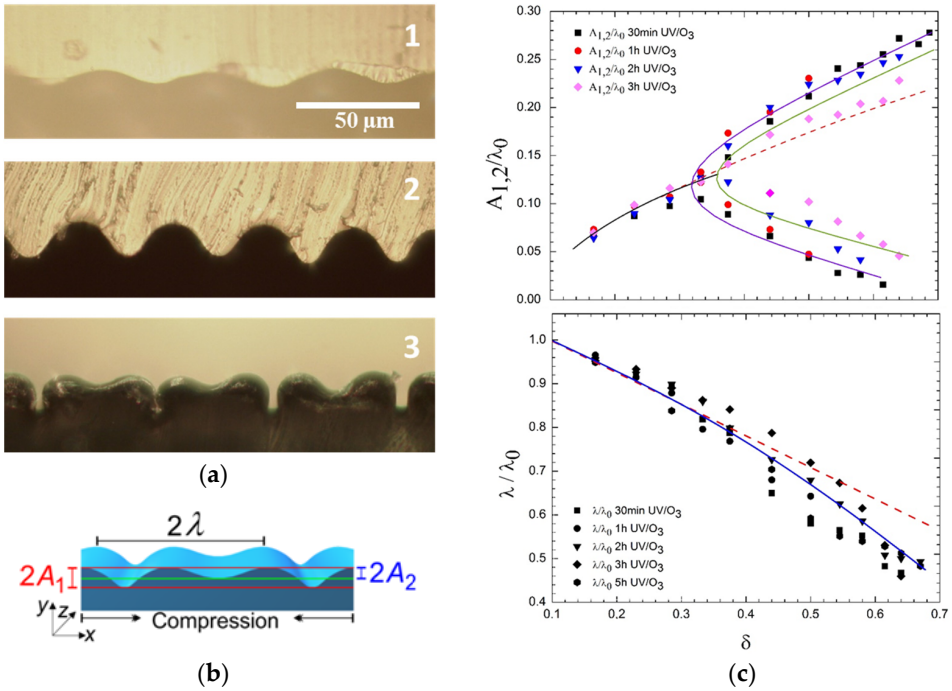

Figure 2. (**a**) Optical microscopy images of thin stiff PDMS film resting on a thick soft PDMS foundation, the PDMS foundation is cured with UV/ozone which modifies the elastic properties of its surface; (**b**) The system composed by the stiff film and the soft foundation is compressed uniaxially along the horizontal *x*-axis. The wavelength and amplitudes of the wrinkles are measured for successive values of the relative compression δ; (**c**) amplitudes, A_1 and A_2, and wavelength, λ, as a function of the compression ratio δ.

Superhydrophobic surfaces are determined by both chemical composition and a dual roughness at both micrometer and nanometer scales. The roughness of hydrophobic surfaces might lead to two states: Wenzel and Cassie-Baxter states.

The Wenzel state [30,31] describes a liquid in contact with the whole structured solid surface and therefore displaying low contact angle and high hysteresis. This state assumed that the liquid completely wets the grooves of the rough surface. The Wenzel state describes homogenous wetting by the relation:

$$\cos\theta_w = r\cos\theta_e \quad (2)$$

where θ_w and θ_e are the Wenzel contact angle and the Young contact angle, respectively, and r is the roughness factor defined as the ratio of the true area of the solid-liquid to its projected area.

The Cassie-Baxter state describes a liquid which is resting partly on the features of a solid material and bridging air between these features [32,33]. The relation between the apparent contact angle θ_c and the equilibrium angle θ_e is described as:

$$\cos\theta_c = -1 + \Phi_s\,(1 + \cos\theta_e) \quad (3)$$

where Φ_s is the area fraction of the projected wet area.

We used the wrinkled topography of the surfaces, as shown before, to study the wettability of surfaces where the wavelength and the amplitude of wrinkles can be conveniently regulated by varying the time of treatment with UV/ozone, the module of elasticity and the applied strain level. By adjusting these parameters, it is possible to get surfaces with very large roughness.

We measured the angle of 1 µL water drop on the molded surface in different cases. First, on the smooth, non-structured surface of PDMS, the equilibrium contact angle was $\theta_e = 110^\circ$ (Figure 3a).

For small compression (δ = 33%), we obtained a wrinkled surface, the apparent contact angle increased to 135° and the liquid penetrated into the surface roughness (Figure 3b), corresponding with the Wenzel state. By adding some stress (δ = 45%), two peak amplitudes of wrinkle appeared and the contact angle increased to θ_w = 145° (Figure 3c), corresponding with the Wenzel state. Increasing the compression ratio (δ = 64%), the apparent contact angle strongly increased and reached values close to 180°, corresponding to the Cassie state (Figure 3d).

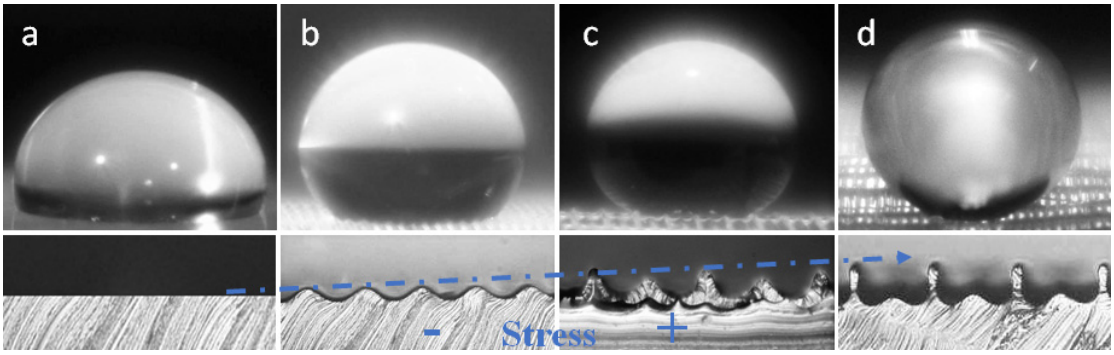

Figure 3. Lateral view images of water droplet on the various surfaces. (**a**) Smooth PDMS (θ_e = 110°); (**b**) sinusoidal wrinkled PDMS (δ = 33% and θ_w = 135°); (**c**) two peak amplitudes of wrinkle (δ = 45% and θ_w = 145°); and (**d**) structured PDMS (δ = 64% and θ_c ~ 180°).

Figure 4 shows the evolution of cos(θ) as a function of the roughness coefficient (δ + 1). The observed points (●) for low/high roughness correspond to both the Wenzel and Cassie models. For low compression (δ < 0.4), the profile of the surface is sinusoidal. We observe an evolution of cos(θ) with a slope equal to 0.4; these results are in agreement with the Wenzel model (blue line in Figure 4). The theoretical line is obtained from Equation (2), where the roughness factor $r \approx \delta + 1$ and the equilibrium contact angle θ_e = 110°. When the compression ratio increases (0.4 < δ < 0.6), the profile of wrinkles evolves progressively from sinusoidal morphology to a more complex pattern characterized by a doubled wavelength. The evolution of the apparent angle as a function of the roughness coefficient shows that we reach an intermediate state in between the Wenzel and the Cassie states. This corresponds to a transition regime between these two extreme states. For higher compression ratio (δ > 0.6), the structure of the surface is characterized by a succession of identical "pillars" with a wavelength 2λ and a larger amplitude (Figure 4). The ratio between the amplitude and the wavelength becomes larger than 1/3. In this case, the droplet of water stays above the surface of wrinkles and pockets of air are easily trapped below it. We thus obtain large contact angles close to 180°. These results correspond to the theoretical line (red line) of the Cassie model (Figure 4). This theoretical curve is computed from Equation (3), by assuming that the area fraction $\Phi_S = \sigma/\lambda$, where σ is the width of the pillars and λ is the length between two consecutive pillars. In order to confirm superhydrophobicity in this case, we measured the tilt angle (at which the drop of water rolled off) and it was less than 3°.

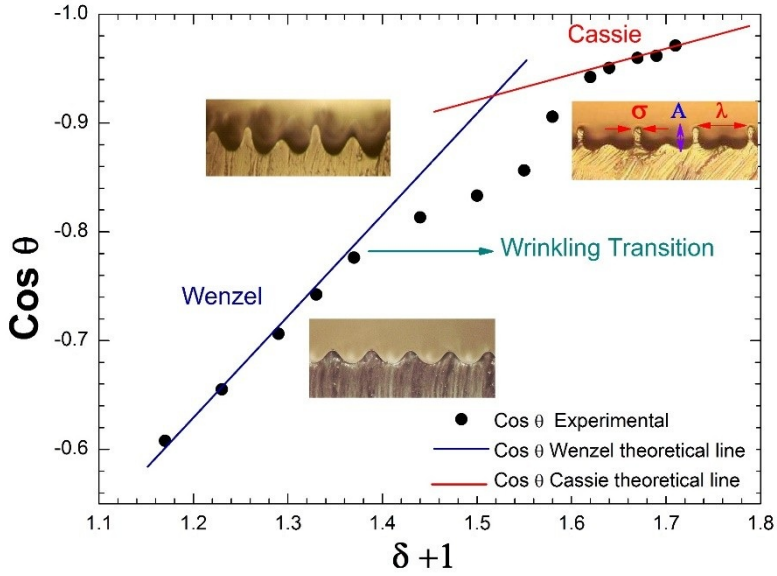

Figure 4. The contact angle *versus* the roughness coefficient. The points (●) are experimental results from the simulations, while the blue line is the theoretical Wenzel line and the red line is the theoretical Cassie line.

4. Conclusions

It is known that the wettability of a surface can be easily modified by adjusting the roughness. The molecules of PDMS have a low surface energy; the value of the contact angle is $\theta_e \sim 110^\circ$. By micro-structuring of PDMS surface, we obtain contact angles significantly larger than 110°. We can control the surface morphology by changing the exposure time to UV/Ozone radiation, the modulus of the PDMS and the compression ratio. By increasing the compression ratio, we observe a transition from the Wenzel state $120^\circ < \theta < 150^\circ$ to the Cassie-Baxter state $\theta > 150^\circ$. These micro-structures characterizing the PDMS surface are similar to those observed on lotus leaves. The superhydrophobic surfaces presented above should also be characterized as self-cleaning.

Author Contributions: A.S., P.D. designed the experiments; A.S. carried out the experiments; A.S., A.Y. and P.D. worked on the theoretical model; A.S., A.Y. and P.D. wrote the manuscript.

Conflicts of Interest: The authors declare no conflict of interest.

Abbreviations

The following abbreviations are used in this manuscript:

PDMS	poly-dimethylsiloxane
UV	Ultra Violet
SEM	Scanning Electron Microscope

References

1. Öner, D.; McCarthy, T.J. Ultrahydrophobic surfaces. Effets of topography length scales on wettability. *Langmuir* **2000**, *16*, 7777–7782. [CrossRef]
2. Bico, J.; Marzolin, C.; Quéré, D. Pearl drops. *Europhys. Lett.* **1999**, *47*, 220–226. [CrossRef]
3. Ditsche-Kuru, P.; Schneider, E.; Melskotte, J.-E.; Brede, M.; Leder, A.; Barthlott, W. Superhydrophobic surfaces of the water bug *Notonecta glauca*: A model for friction reduction and air retention. *Beilstein J. Nanotechnol.* **2011**, *2*, 137–144. [CrossRef] [PubMed]
4. Cerman, Z.; Striffler, B.F.; Barthlott, W. Dry in the water: The superhydrophobic water fern Salvinia—A model for biomimetic surfaces. In *Functional Surfaces in Biology: Little Structures with Big Effects*; Gorb, S.N., Ed.; Springer: Dordrecht, The Netherlands, 2009; Volume 1, pp. 97–111.

5. McHale, G.; Newton, M.I.; Shirtcliffe, N.J. Immersed superhydrophobic surfaces: Gas exchange, slip and drag reduction properties. *Soft Matter* **2010**, *6*, 714–719. [CrossRef]
6. Awada, H.; Grignard, B.; Jérôme, C.; Vaillant, A.; de Coninck, J.; Nysten, B.; Jonas, A.M. Correlation between Superhydrophobicity and the Power Spectral Density of Randomly Rough Surfaces. *Langmuir* **2010**, *26*, 17798–17803. [CrossRef] [PubMed]
7. Shin, S.; Seo, J.; Han, H.; Kang, S.; Kim, H.; Lee, T. Bio-Inspired Extreme Wetting Surfaces for Biomedical Applications. *Materials* **2016**, *9*, 116. [CrossRef]
8. Bowden, N.; Huck, W.; Paul, K.; Whitesides, G.M. The Controlled Formation of Ordered, Sinusoidal Structures by Plasma Oxidation of an Elastomeric Polymer. *Appl. Phys. Lett.* **1999**, *75*, 2557–2559. [CrossRef]
9. Park, J.; Hammond, P. Polyelectrolyte multilayer formation on neutral hydrophobic surfaces. *Macromolecules* **2005**, *38*, 10542–10550. [CrossRef]
10. Roucoules, V.; Ponche, A.; Geissler, A. Changes in silicon elastomeric surface properties under stretching induced by three surface treatments. *Langmuir* **2007**, *23*, 13136–13145. [CrossRef] [PubMed]
11. Brassard, J.-D.; Sarkar, D.; Perron, J. Fluorine Based Superhydrophobic Coatings. *Appl. Sci.* **2012**, *2*, 453–464. [CrossRef]
12. Graubner, V.; Jordan, R.; Nuyken, O.; Schnyder, B.; Lippert, T.; Kotz, R.; Wokaun, A. Photochemical modification of cross-linked poly(dimethylsiloxane) by irradiation at 172 nm. *Macromolecules* **2004**, *37*, 5936–5943. [CrossRef]
13. Lin, P.-C.; Yang, S. Mechanically switchable wetting on wrinkled elastomers with dual-scale roughness. *Soft Matter* **2009**, *5*, 1011–1018. [CrossRef]
14. Cerda, E.; Ravi-Chandar, K.; Mahadevan, L. Thin films: Wrinkling of an elastic sheet under tension. *Nature* **2000**, *419*, 579–580. [CrossRef] [PubMed]
15. Pipe, C.; McKinley, G.H. Microfluidic rheometry. *Mech. Res. Commun.* **2009**, *36*, 110–120. [CrossRef]
16. Galindo-Rosales, J.; Alves, A.; Oliveira, N. Microdevices for extensional rheometry of low viscosity elastic liquids: A review. *Microfluid. Nanofluid.* **2013**, *14*, 1–19. [CrossRef]
17. Haward, J. Microfluidic extensional rheometry using stagnation point flow. *Biomicrofluidics* **2016**, *10*, 043401. [CrossRef] [PubMed]
18. Broboana, D.; Tanase, O.N.; Balan, C. Influence of patterned surface in the rheometry of simple and complex fluids. *J. Non-Newton. Fluid Mech.* **2015**, *222*, 151–162. [CrossRef]
19. Roman, S.V.; Dimitrios, V.P. Review of Fluid Slip over Superhydrophobic Surfaces and Its Dependence on the Contact Angle. *Ind. Eng. Chem. Res.* **2008**, *47*, 2455–2477.
20. Song, D.; Daniello, R.; Rothstein, J. Drag reduction using superhydrophobic sanded Teflon surfaces. *Exp. Fluids* **2014**, *55*, 1783. [CrossRef]
21. Farokhirad, S.; Morris, J.; Lee, T. Coalescence-induced jumping of droplet: Inertia and viscosity effects. *Phys. Fluids* **2016**, *27*, 102102. [CrossRef]
22. Zhang, X.; Wang, L.; Levänen, E. Superhydrophobic surfaces for the reduction of bacterial adhesion. *RSC Adv.* **2013**, *3*, 12003–12020. [CrossRef]
23. Brau, F.; Vandeparre, H.; Sabbah, A.; Poulard, C.; Boudaoud, A.; Damman, P. Multiple-length-scale elastic instability mimics parametric resonance of nonlinear oscillators. *Nat. Phys.* **2011**, *7*, 56–60. [CrossRef]
24. Efimenko, K.; Rackaitis, M.; Manias, E.; Vaziri, A.; Mahadevan, L.; Genzer, J. Nested self-similar wrinkling patterns in skins. *Nat. Mater.* **2005**, *4*, 293–297. [CrossRef] [PubMed]
25. Genzer, J.; Efimenko, K. Recent developments in superhydrophobic surfaces and their relevance to marine fouling: A review. *Biofouling* **2006**, *22*, 339–360. [CrossRef] [PubMed]
26. Stafford, C.; Harrison, C.; Beers, K.; Karim, A.; Amis, E.; Vanlandingham, M.; Kim, H.; Volksen, W.; Miller, R.; Simonyi, E. A buckling-based metrology for measuring the elastic moduli of polymeric thin films. *Nat. Mater.* **2004**, *3*, 545–550. [CrossRef] [PubMed]
27. Vandeparre, H.; Damman, P. Wrinkling of Stimuloresponsive Surfaces: Mechanical Instability Coupled to Diffusion. *Phys. Rev. Lett.* **2008**, *101*, 124301. [CrossRef] [PubMed]
28. Kolaric, B.; Vandeparre, H.; Desprez, S.; Vallée, R.; Damman, P. *In situ* tuning the optical properties of a cavity by wrinkling. *Appl. Phys. Lett.* **2010**, *96*, 043119. [CrossRef]
29. Odijk, T. Microfibrillar buckling within fibers under compression. *J. Chem. Phys.* **1998**, *108*, 6923–6928. [CrossRef]
30. Wenzel, R.N. Resistance of solid surface to wetting by water. *Ind. Eng. Chem.* **1936**, *28*, 988–994. [CrossRef]

31. Wenzel, R.N. Surface roughness and contact angle. *Phys. Colloid Chem.* **1949**, *53*, 1466–1467. [CrossRef]
32. Cassie, A.B.; Baxter, S. Large Contact Angles of Plant and Animal Surfaces. *Nature* **1945**, *155*, 21–22. [CrossRef]
33. Cassie, A.B. Contact angles. *Discuss. Faraday Soc.* **1948**, *3*, 11–14. [CrossRef]